Journal of Thermal Science Vol.24, No.4 (2015) 344–349

DOI: 10.1007/s11630-015-0793-z **Article ID: 1003-2169(2015)04-0344-06**

Effect of Nozzle Inlet Shape on Annular Swirling Flow with Non-Equilibrium Condensation

Yusuke FUKUSHIMA[1], Shigeru MATSUO[2], Toshiaki SETOGUCHI[3], Norimasa SHIOMI[4], Tokitada HASHIMOTO[5], Heuy Dong KIM[6], and Shen YU[7]

1. Graduate School of Science & Engineering, Saga University, 1, Honjo-machi, Saga-shi, Saga 840-8502, Japan
2. Department of Advanced Technology Fusion, Saga University, 1, Honjo-machi, Saga-shi, Saga 840-8502, Japan
3. Institute of Ocean Energy, Saga University, 1, Honjo-machi, Saga-shi, Saga 840-8502, Japan
4. Department of Mechanical Engineering, Saga University, 1, Honjo-machi, Saga-shi, Saga 840-8502, Japan
5. Department of Advanced Technology Fusion, Saga University, 1, Honjo-machi, Saga-shi, Saga 840-8502, Japan
6. School of Mechanical Engineering, Andong National University, 388, Songchun-dong, Andong 760749, Korea
7. Institute of Engineering Thermophysics, Chinese Academy of Science, P.O. Box 2706, Beijing 100080, China

Recently, by combining a swirl flow with non-equilibrium condensation phenomena of condensate gas generated in a supersonic flow, a separating and extracting techniques of condensate gas have been developed. This technique can reduce the size of the device and don't use chemicals. In the present study, by using a non-equilibrium condensation phenomenon of moist air occurred in the supersonic flow in the annular nozzle composed of an inner body and an outer nozzle with a swirl, the possibility of separation of the condensable gas and the effect of shape of nozzle inlet on the flow field were examined numerically.

Keywords: compressible flow, non-equilibrium condensation, supersonic annular nozzle, swirl flow, simulation

Introduction

In recent years, we human beings are faced with resolution of environmental issues and the sophistication of the energy structure on a global scale. It is considered that natural gas of lower CO_2 emissions in such a situation is important as an alternative energy of coal and petroleum [1].

The separation and extraction of condensate gas contained in the natural gas is important for natural gas processing. Recently, separating and extracting technologies of condensate gas have been developed by using a swirling flow in a supersonic annular nozzle

It is known from the previous research [2, 3, 4] that a rapid expansion of moist air or steam in a supersonic nozzle gives rise to a non-equilibrium condensation. If the latent heat released by condensation exceeds a certain quantity, a condensation shock wave occurs in the flow field [2, 5]. Such a non - equilibrium condensation may occur in the supersonic annular nozzle used in the separating and extracting technologies of condensate gas. The technology which uses the swirling flow and non - equilibrium condensation, has the advantages of reduction of the device size and not using chemical substance.

However, the detailed flow information for non - equilibrium condensation in the supersonic annular nozzle is not well known yet and there are many unresolved problems for performance of the separation and extraction.

Received: May 2015
Shigeru MATSUO: Professor

Nomenclature

a	nozzle opening angle (degree)	**Greek symbols**	
D	diameter (mm)	δ^*	displacement thickness (mm)
G	radial distribution ratio of liquid phase (-)	ν	kinematic viscosity (m^2/s)
g	condensate mass fraction (-)	ρ	density (kg/m^3)
p	pressure (kPa)		
r	radius (mm)	**Subscripts**	
S	degree of supersaturation (-)	0	stagnation point
$S_{w,in}$	swirl number at inlet (-)	in	inner
T	temperature (K)	out	outer
u, v, w	velocity components (m/s)		
x, y, z	Cartesian coordinates (mm)		

Especially, effect of device configuration on the flow field is not clarified including the operating principle.

Therefore it is necessary to research further in order to improve the efficiency of the equipment.

In the present study, by using a non-equilibrium condensation phenomenon of moist air occurred in the supersonic flow in the annular nozzle with a swirl, the effect of the nozzle inlet shape on spatial distribution of ties of the condensable gas separation and device size reduction is shown qualitatively.

Experimental Apparatus and Method

An experimental work was conducted to evaluate the validity of the present calculation method in case of no swirl. Figure 1 shows a schematic diagram of experimental apparatus. A supersonic indraft wind tunnel where the moist air at atmospheric pressure was drawn into a vacuum tank, was used in the present experiment.

Figure 2 shows details of test section. An annular nozzle is composed of an inner body and an outer nozzle. The outer nozzle is coaxial with the inner body. Throat diameter of the outer nozzle in case of no inner body is D_e = 30 mm and design Mach number at the nozzle exit is 3.0. The pressure measurements were conducted by some semiconductor pressure transducers (Kulite XT-190) mounted on 10 pressure holes (diameter 1.0 mm) along the outer wall as shown in Fig.2.

The stagnation pressure p_0 and temperature T_0 of moist air in the reservoir are 99.8 kPa and 300 K, respectively. The values of initial degree of supersaturation S_0, which is the ratio of vapor pressure to the equilibrium saturation pressure corresponding to the inlet temperature, are 0.25 and 0.70.

Numerical Analysis

Assumptions of the two phase flow are as follows; both velocity slip and temperature difference don't exist between condensate particles and gas mixture, and the effect of the condensate particles on pressure is neglected.

The governing equations used in the present study are the 3D compressible Navier-Stokes equations combined with equations of continuity, energy, turbulent kinetic energy, specific dissipation rate, conservation of mass of the liquid phase and conservation of the number density of droplets. To estimate the eddy viscosity, k-ω model was employed in computations [6].

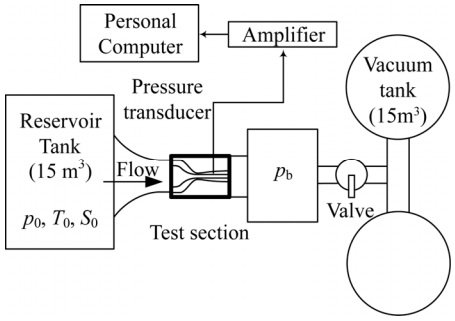

Fig. 1 Experimental apparatus.

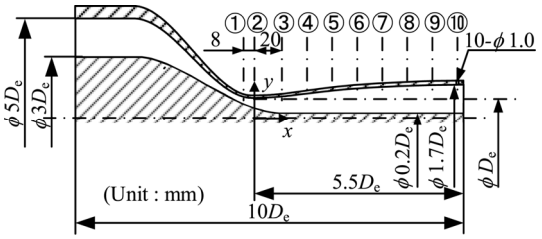

Fig. 2 Supersonic nozzle with inner body (D_e = 30 mm).

The governing equations were discretized in space using a cell-centered finite volume formulation with a quadrilateral structured cell system and using the Euler implicit method in time [7]. Furthermore, a third-order accurate MUSCL TVD scheme based on Roe's approximate Riemann solver was applied to the inviscid fluxes

and the viscous fluxes were evaluated by first-order accurate central differences method. Generation terms associated with turbulence and condensation were evaluated by first-order accurate central differences method. Unfactored implicit equations derived with no approximate factorization were solved by a point Gauss-Seidel relaxation method [8].

Figure 3 shows three types of nozzle geometry used in this calculation (Cases A, B, C). An annular nozzle in Fig.3(a) is composed of an inner body and an outer nozzle. The outer nozzle is coaxial with the inner body. Throat diameter of the outer nozzle in case of no inner body is D = 10 mm which is the same as one at the nozzle exit. The nozzle opening angle a is 4°. Design Mach number is 2.24. In Cases A (Fig.3(b)), B (Fig.3(c)) and C (Fig.3(d)), nozzle shapes downstream of x = -0.46D are the same. Inlet shapes of Cases B and C were designed to become larger than angular momentum of Case A. For Case A, outer inlet radius r_{out} is 2D, inner inlet radius r_{in} is 1.75D. r_{out} and r_{in} of Case B are larger than those of Case A and values of inlet closs-sectional area of the flow path for Cases A and B are equal. The inlet closs-sectional area of Case C is half of that of Case A. r_i for each figure is given as

$$r_i = \sqrt{(r_{in}^2 + r_{out}^2)/2} \tag{1}$$

where r_i means the position of the radius corresponding to half of annular area at the inlet.

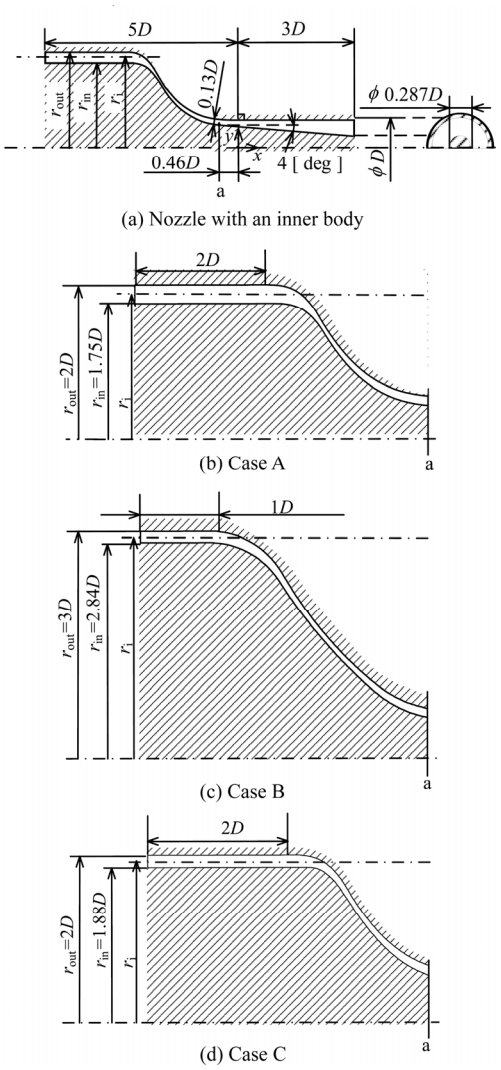

Fig. 3 Nozzle geometry (D = 10 mm).

Figure 4 shows a computational domain of the supersonic annular flow field and boundary conditions. The adiabatic no-slip wall was used as boundary condition. Inflow condition was fixed at initial condition. Outflow condition is a zero-order extrapolation. Periodic boundary conditions were imposed for conservative variables. Condensate mass fraction g was set at g = 0 on the wall. The cell density in the structured - grid region is 210× 80×30.

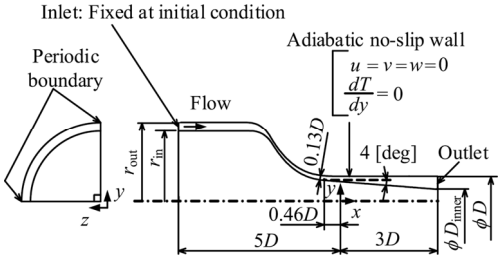

Fig. 4 Computational domain and boundary conditions.

Table 1 shows calculation conditions for Cases A, B and C in the present calculation. Stagnation pressure p_0 and temperature T_0 at stagnation point are 101.3 kPa and 293 K, respectively. The initial degrees of supersaturation S_0 of moist air are 0 and 0.8. Swirl numbers at the inlet were set at 0 and 2.0.

Table 1 Initial conditions.

(1) Case A.

p_0 [kPa]	T_0 [K]	D [mm]	r_{in} [-]	r_{out} [-]	S_0 [-]	$S_{w,in}$ [-]
101.3	293	10	1.75D	2D	0	0
						2.0
					0.8	0
						2.0

(2) Case B.

p_0 [kPa]	T_0 [K]	D [mm]	r_{in} [-]	r_{out} [-]	S_0 [-]	$S_{w,in}$ [-]
101.3	293	10	2.84D	3D	0	0
						2.0
					0.8	0
						2.0

(3) Case C.

p_0 [kPa]	T_0 [K]	D [mm]	r_{in} [-]	r_{out} [-]	S_0 [-]	$S_{w,in}$ [-]
101.3	293	10	1.88D	2D	0	0
						2.0
					0.8	0
						2.0

Results and Discussions

Figure 5 shows static pressure distributions on the outer wall for dry air (S_0=0.25) and moist air (S_0=0.70) in case of no swirl ($S_{w,in}$=0). In this figure, comparison between the experimental and simulated static pressure distributions are shown and it is found that simulated results agree well with experimental results qualitatively.

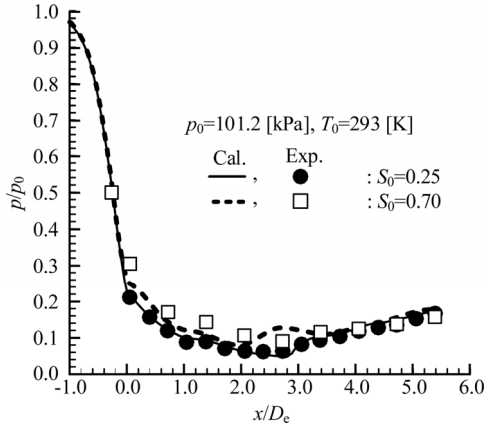

Fig. 5 Distributions of static pressure on the outer wall ($S_{w,in}$ = 0).

Figures 6(a), 6(b) and 6(c) show contour maps of condensate mass fraction g and sonic line for Cases A, B and C, respectively (S_0 = 0.8). In each figure, simulated results for $S_{w,in}$=0 and 2.0 are shown including the onset of condensation. As seen from each case, positions of sonic line and onset of condensation move upstream in case of swirling flow ($S_{w,in}$=2.0) and this tendency appears particularly in the range close to the inner side significantly. Furthermore, sonic line and onset of condensation for Cases B and C with large angular momentum at the inlet are located upstream compared with those of Case A.

Figures 7(a) and 7(b) show distributions of condensate mass fraction g and static pressure p in the cross section at the position of x/D=0 in cases of $S_{w,in}$=0 and 2.0, respectively. In case of the flow with swirl ($S_{w,in}$=2.0), decrease of static pressure is clearly observed in the range close to the inner side. This means that the flow with swirl expand rapidly on the inner side. As a result, non-equilibrium condensation is more likely to occur compared to the case of no swirl ($S_{w,in}$=0). Further, con densate mass fraction for Case C becomes the largest on the inner side.

In order to investigate the amount of condensate in the range of the outer wall side in the annular nozzle, a new function defined by the following equation was introduced.

$$G = \int_{y=r_i}^{y_{outer}} 2\pi g \rho u r \mathrm{d}r \Big/ \int_{y_{inner}}^{y_{outer}} 2\pi g \rho u r \mathrm{d}r \qquad (2)$$

where G (radial distribution ratio of liquid phase) shows ratio of integrated value of mass flow rate of the liquid phase from $y=r_i$ to outer wall to integrated value of massflow rate of the liquid phase from inner wall to outer wall in the cross section in the annular nozzle channel perpendicular to the x-axis.

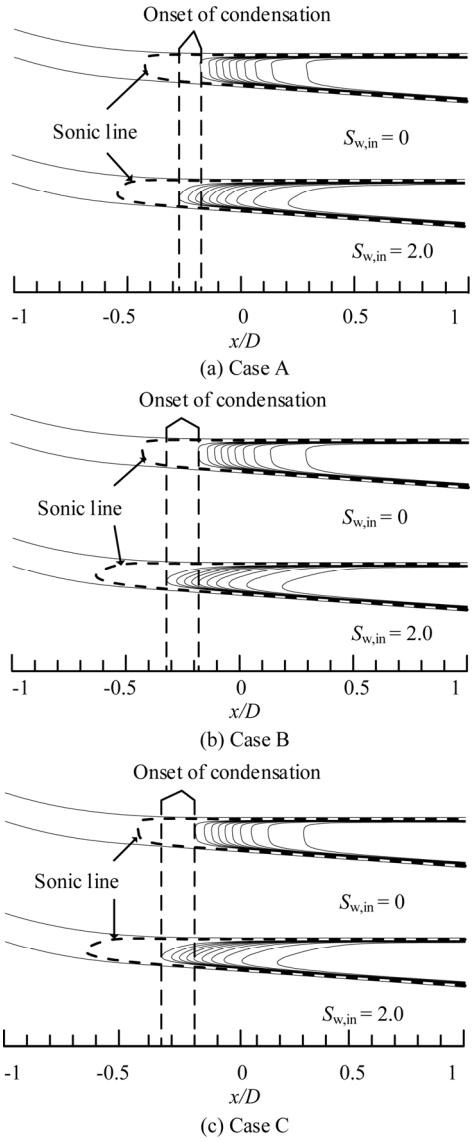

Fig. 6 Contour maps of g and sonic line (S_0 = 0.8).

Figure 8 shows distributions of G along x-axis for no swirling flow ($S_{w,in}$= 0) and swirling flow ($S_{w,in}$ = 2.0) for Cases A, B and C (S_0 = 0.8). In downstream of the annular nozzle, G in case with swirl for each case becomes large in comparison with cases of no swirling flows. This means that the condensate gathers toward the outer wall side compared to cases of no swirling flows. In particular, in case of Case C with swirl ($S_{w,in}$ =2.0), value of G becomes the largest at the exit. Furthermore, the positions for Cases B and C with swirl ($S_{w,in}$ = 2.0) with the same one as the value at the nozzle exit for Cases A and B ($S_{w,in}$ = 0) is located upstream from the nozzle exit. This shows possibility of miniaturization of equipment.

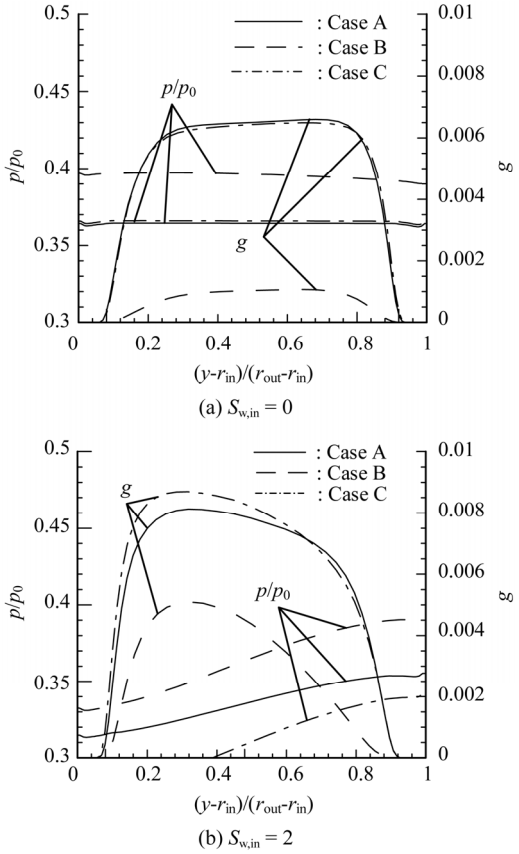

Fig. 7 Distributions of g and p (S_0=0.8, x/D=0).

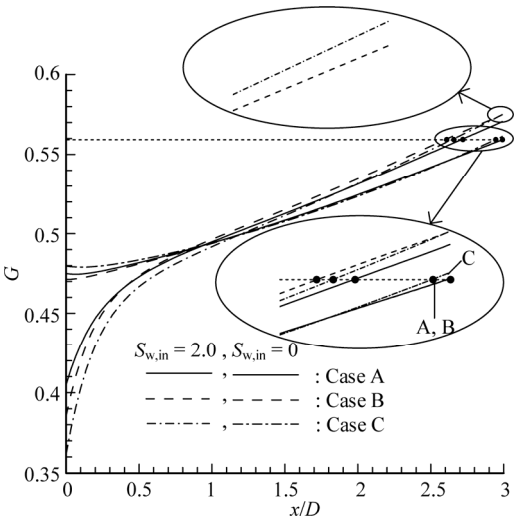

Fig. 8 Distributions of G (S_0 = 0.8).

Figure 9 show distributions of displacement thickness of boundary layer δ^* on the inner and outer walls for Case C (S_0=0.8). From this figure, it is found that the displacement thickness in the case with swirl becomes thick in the inner wall side and thin in the outer wall side in comparison with the case without swirl. Results of Cases A and B were in the same manner as the tendency of Case C.

Figure 10 shows distributions of dynamic viscosity ν in cross-section at x/D = 3 (Case C, S_0=0.8). As seen from this figure, there are little differences between cases with swirl and without swirl on the outer wall side and the dynamic viscosity becomes large on the inner wall side in case with swirl compared with that of no swirl. As a result, it is considered that displacement thickness becomes thin at the outer wall side and thick at the inner wall side as shown in Fig.9. Changes of dynamics viscosity for Cases A and B were in the same manner as the tendency of Case C.

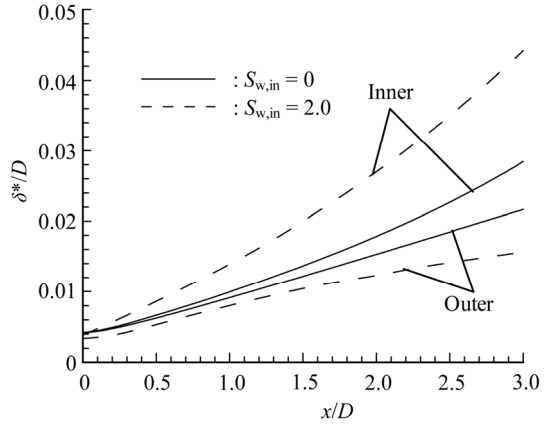

Fig. 9 Distributions of displacement thickness (Case C, S_0 = 0.8).

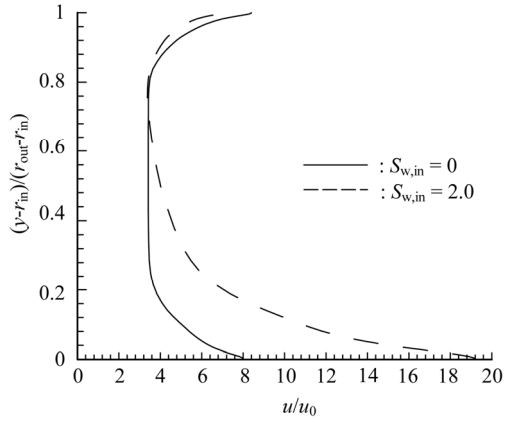

Fig. 10 Distributions of kinetic viscosity (Case C, S_0 = 0.8, x/D = 3).

For the cause of the distributions of G in Fig.8, it is considered from these results as follows. Non - equilibrium condensation in the outer wall side occurs in the range closer to the outer wall in case with swirl because the boundary layer on the outer wall becomes thin. On the other hand, the condensation in the inner wall side occurs in the range away from the inner wall in comparison with the case of no swirl because the boundary layer at the inner side becomes thick.

Conclusions

A numerical study has been performed to investigate

the effect of the nozzle inlet shape on spatial distribution of condensate, possibilities of the condensable gas separation and device size reduction was investigated qualitatively. The results obtained are summarized as follows.

(1) The positions of sonic line and onset of condensation in the annular nozzle moved upstream in case with a swirling flow and this tendency appeared particularly in the range close to the inner wall side significantly.

(2) The displacement thickness of boundary layer in the case with swirl became thick in the inner wall side and thin in the outer wall side in comparison with the case without swirl.

(3) In downstream of the annular nozzle with the same nozzle inlet shape, the radial distribution ratio of liquid phase in the range of the outer side in case with swirl became large in comparison with the case of no swirl.

(4) The radial distribution ratio of liquid phase became large with an increase of angular momentum at the nozzle inlet in the case of the same swirl number.

(5) There is a possibility that the swirling flow with large angular momentum contributes to miniaturization of the equipment.

Acknowledgements

This work was supported by JSPS KAKENHI Grand number 26420116.

References

[1] Kaneko, H., (2007), Liquefied petroleum gas supply and demand perspective and LP gas synthesis technology development, Journal of the Japan Institute of Energy, Vol.86, No.4, pp.232−237.

[2] Wegener, P.P., Mach, L.M., (1958), Condensation in supersonic and hypersonic wind tunnels, Advances in applied mechanics, Vol.5, pp.307−447.

[3] Prast, B., Lammers, B., Betting, M., (2006), CFD for supersonic gas processing, The 5th international conference on CFD in the process industries, Melbourne, Australia, pp.1−6.

[4] Wen, C., Cao, X., Yang, Y., Zhang, J., (2012), Evaluation of natural gas dehydration in supersonic swirling separators applying the discrete particle method, advanced powder technology, Vol.23 No.2, pp.228−233.

[5] Matsuo, K., Kawagoe, S., Sonoda, K. and Sakao, K., (1985), Studies of Condensation Shock Waves (Part1, Mechanism of their Formation), Bulletin of JSME, Vol.28, No. 241, pp.1416−1422.

[6] Wilcox, D.C., (2008), Formulation of the k-ω turbulence model revisited, AIAA Journal, Vol.46, No.11, pp.2823−2838.

[7] Furukawa, M., Nakano, T., Inoue, M., (1992), Unsteady Navier-Stokes simulation of transonic cascade flow using an unfactored implicit upwind relaxation scheme with inner iterations, Transactions of the ASME, Journal of Turbomachinery, Vol.114, No.3, pp.599−606.

[8] Chakravarthy, S.P., (1984), Relaxation methods for unfactored implicit upwind schemes, AIAA paper, Reno Nevada, USA, 84-0165.